Applied Catalysis B: Environmental 88 (2009) 315–322

Contents lists available at ScienceDirect

Applied Catalysis B: Environmental

journal homepage: www.elsevier.com/locate/apcatb

Carbon nanotube-supported Pd–ZnO catalyst for hydrogenation of CO_2 to methanol

Xue-Lian Liang, Xin Dong, Guo-Dong Lin, Hong-Bin Zhang *

Department of Chemistry, College of Chemistry and Chemical Engineering; State Key Laboratory of Physical Chemistry for Solid Surfaces and National Engineering Laboratory for Green Chemical Productions of Alcohols-Ethers-Esters, Xiamen University, Xiamen 361005, China

ARTICLE INFO

Article history:
Received 11 July 2008
Received in revised form 22 September 2008
Accepted 4 November 2008
Available online 24 November 2008

Keywords:
Carbon nanotubes
CNT-supported Pd–ZnO catalyst
CO_2 hydrogenation
Methanol synthesis

ABSTRACT

A type of Pd–ZnO catalysts supported on multi-walled carbon nanotubes (MWCNTs) were developed, with excellent performance for CO_2 hydrogenation to methanol. Under reaction conditions of 3.0 MPa and 523 K, the observed turnover-frequency of CO_2 hydrogenation reached 1.15×10^{-2} s^{-1} over the 16%$Pd_{0.1}Zn_1$/CNTs(*h-type*). This value was 1.17 and 1.18 times that (0.98×10^{-2} and 0.97×10^{-2} s^{-1}) of the 35%$Pd_{0.1}Zn_1$/AC and 20%$Pd_{0.1}Zn_1$/γ-Al_2O_3 catalysts with the respective optimal $Pd_{0.1}Zn_1$-loading. Using the MWCNTs in place of AC or γ-Al_2O_3 as the catalyst support displayed little change in the apparent activation energy for the CO_2 hydrogenation, but led to an increase of surface concentration of the Pd^0-species in the form of PdZn alloys, a kind of catalytically active Pd^0-species closely associated with the methanol generation. On the other hand, the MWCNT-supported Pd–ZnO catalyst could reversibly adsorb a greater amount of hydrogen at temperatures ranging from room temperature to 623 K. This unique feature would help to generate a micro-environment with higher concentration of active H-adspecies at the surface of the functioning catalyst, thus increasing the rate of surface hydrogenation reactions. In comparison with the "Parallel-type (*p-type*)" MWCNTs, the "Herringbone-type (*h-type*)" MWCNTs possess more active surface (with more dangling bonds), and thus, higher capacity for adsorbing H_2, which make their promoting action more remarkable.

1. Introduction

Hydrogenation of carbon dioxide has been considered as one of the most economical and effective ways to chemically fix huge amount of emitted CO_2. In order to improve climate conditions, it is desirable to develop methods to convert CO_2 into valuable chemicals. Among the options considered, catalytic hydrogenation of CO_2 to produce methanol has received much attention. A number of Cu-based catalysts, especially CuO–ZnO-based catalysts modified with different metals or oxides, for methanol synthesis via CO_2 hydrogenation have been reported [1–8]. Supported Pd catalysts have also been found to exhibit considerable activity and selectivity for hydrogenation of CO_2 to methanol, and the supporter has significant effect on the performance of the catalyst [9–12].

To the other front, multi-walled carbon nanotubes (MWCNTs), as a novel nanocarbon material, have been drawing increasing attention recently [13–15]. This new form of carbon is structurally close to hollow graphite fiber, except that it has a much higher degree of structural perfection. MWCNTs possess several unique features, such as graphitized tube-wall, nanometer-sized channel and sp^2-C-constructed surface. They display high thermal/electrical conductivity, medium to high specific surface areas, and excellent performance for adsorption of hydrogen, all of which render this kind of nanostructured carbon materials full of promise as a novel catalyst support and/or promoter.

Here we report the development of a type of MWCNT-supported Pd–ZnO catalysts, which display much better performance for highly effective and selective formation of methanol from CO_2 hydrogenation, in comparison with the reference Pd–ZnO catalysts supported on alumina (γ-Al_2O_3) and activated carbon (AC).

2. Experimental

2.1. Catalyst preparation

A "Herringbone-type" MWCNTs (symbolized as "CNTs(*h-type*)" and simplified as "CNTs" in later text, unless otherwise specified) were prepared from catalytic decomposition of CH_4 by the catalytic method reported previously [16]. The freshly prepared CNTs were purified with treatment of boiling nitric acid (~8 mol/L, at 363 K)

* Corresponding author. Tel.: +86 592 2184591; fax: +86 592 2184591.
E-mail address: hbzhang@xmu.edu.cn (H.-B. Zhang).

0926-3373/$ – see front matter © 2008 Elsevier B.V. All rights reserved.
doi:10.1016/j.apcatb.2008.11.018

for 8 h, followed by rinsing with de-ionized water twice, and then drying at 383 K under N_2-atmosphere. Open-end CNTs with somewhat hydrophilic surface were then obtained. For comparison, a "Parallel-type" MWCNTs (symbolized as "CNTs(*p-type*)" in later text) were prepared and purified following the same method as above from catalytic disproportionation of CO [16].

A series of Pd–ZnO catalysts supported on the CNTs, denoted as *x*%(mass percentage)Pd_iZn_j/CNTs, were prepared by a stepwise incipient wetness method. An aqueous solution containing desired amount of Zn, which was prepared by dissolving the $Zn(NO_3)_2{\cdot}6H_2O$ (of AR grade, State Pharmaceutical Group Chem. Reagent Co., Ltd.) into a calculated amount of de-ionized water, was impregnated onto the HNO_3-treated CNT-support, followed by drying at 383 K for 10 h and calcining at 573 K under N_2-atmosphere for 2 h. Next, an aqueous solution containing a calculated amount of Pd, which was prepared by dissolving a calculated amount of $PdCl_2$ (of AR grade, Shanghai Inst. of Fine Chem. Materials) to a calculated amount of concentrated hydrochloric acid, was impregnated onto the above Zn-impregnated intermediate, followed by drying at 383 K for 10 h, thus yielding the oxidized precursor of *x*%Pd_iZn_j/CNTs catalyst.

The reference catalysts supported on γ-Al_2O_3 and activated carbon, noted as *x*%Pd_iZn_j/γ-Al_2O_3 and *x*%Pd_iZn_j/AC respectively, were prepared in the similar way. Prior to being used, the γ-Al_2O_3 supporter (Shanghai Chem. Reagent Co., with 217 m^2/g of N_2-BET-SSA) was calcined at 773 K for 3 h. The AC supporter (Xiamen Chem. Reagent Co., with 830 m^2/g of N_2–BET–SSA) was pre-treated first with 10% NaOH aqueous solution and then with 50% HNO_3 solution, followed by rinsing with de-ionized water and drying at 383 K. All samples of catalyst-precursors were pressed, crushed, and sieved to a size of 20–40 mesh for the activity evaluation.

2.2. Catalyst evaluation

The methanol synthesis reaction was carried out in a conventional fixed-bed flow reactor. Prior to the reaction, the sample (0.5 g, 20–40 mesh) of the oxide-precursor of catalyst was pre-reduced *in situ* with a mixture of 5%H_2–95%N_2 at a flow-rate of 3600 ml/(g · h) under atmospheric pressure. The reduction temperature was programmed to rise from room temperature to 773 K, to maintain at that temperature for 6 h, and then to decrease to the desired temperature for the catalyst test. The reaction of CO_2 hydrogenation was conducted at a stationary state under reaction conditions of 503–543 K, 3.0 MPa, $V(H_2):V(CO_2):V(N_2)$ = 69:23:8, $GHSV_{outlet}$ = 1800 ml/(h · g). The product mixtures were analyzed by an on-line gas chromatograph (Model GC-950 by Shanghai Haixin GC Instruments, Inc.) equipped with dual detectors (TCD and FID) and dual columns filled with carbon molecular sieve (TDX-01) and Porapak Q-S (USA), respectively. The former column (1.0 m length) was used for the analysis of N_2 (as internal standard), CO and CO_2, while the latter (2.0 m length) for alcohols, hydrocarbons and oxygenates. CO_2 hydrogenation-conversion (namely the CO_2-conversion after deducting the contribution of reverse-water–gas-shift (RWGS) side-reaction, symbolized as $X(CO_2$-hydr.) in later text) was determined through an internal standard, and the carbon-based selectivity for the hydrogenation products, CH_3OH and hydrocarbons (symbolized as $S(CH_3OH)$ and S(HC) in later text) was calculated by an internal normalization method.

2.3. Catalyst characterization

XRD measurements were carried out on an X'Pert PRO X-ray diffractometer (PANalytical) with Cu Kα (λ = 0.15406 nm) radiation. A continuous scan mode was used to collect 2θ data from 10° to 90°. The voltage and current were 40 kV and 30 mA, respectively. X-ray photoelectron spectroscopy (XPS) measurements were done on a Quantum 2000 Scanning ESCA Microprobe instrument with Al Kα radiation (15 kV, 25 W, $h\nu$ = 1486.6 eV) under ultrahigh vacuum (10^{-7} Pa), calibrated internally by the carbon deposit C(1s) (E_b = 284.7 eV).

Tests of H_2-temperature-programmed desorption (H_2-TPD) of catalyst were conducted on an adsorption/desorption system. 200 mg of catalyst sample was used for each test. Prior to H_2-TPD test, the sample of catalyst-precursor was pre-reduced *in situ* in the TPD equipment by N_2-carried 5%H_2 gaseous mixture stream (900 ml/h) at 773 K for 6 h, and then flushed by an Ar (of 99.999% purity) stream (30 ml/min) at 773 K for 30 min to clean its surface, followed by cooling down to 433 K, switching to a H_2 (of 99.999% purity) stream for hydrogen adsorption at 433 K for 30 min and subsequently at room temperature for 8 h, and then flushing by the Ar stream at room temperature till the stable baseline of GC appeared. The rate of temperature increase was 10 K/min. Change of hydrogen-signal was monitored using an on-line GC (Shimadzu GC-8A) with a TC detector.

Specific surface area (SSA) was determined by N_2 adsorption using a Micromeritics Tristar-3000 system. Measurement of CO chemisorption on the catalysts was performed by a Micromeritics ASAP-2010 Micropore Analyzer. From the determined amount of chemisorbed CO, the dispersion and surface area of metallic palladium were calculated [17]. 0.1–0.2 g of catalyst sample was used for each test. The sample was put into a quartz tube, followed by evacuating for 10 min at 393 K, then switching to a purified H_2 stream (30 ml/min) as reducing gas to conduct an *in situ* H_2-TPR treatment of the catalyst sample, subsequently evacuating for 1 h at the reduction temperature and for 1 h more after cooling down to room temperature, and then switching to gaseous CO (of 99.99% purity) to conduct the measurement of CO chemisorption following the specified procedure of the aforementioned analyzer. The results of blank test showed that under the above-mentioned experimental conditions, the determined amounts of CO chemisorption on the three supports (CNTs, γ-Al_2O_3 and AC) were all zero, indicating that the determined amounts of CO chemisorption on the corresponding supported Pd catalysts were contributed solely by CO chemisorption on the metal Pd surface.

3. Results and discussion

3.1. Optimization of the catalyst composition

3.1.1. PdZn-loading amount

The reaction activity of CO_2 hydrogenation over a series of *x*%$Pd_{0.085}Zn_1$/CNTs catalysts with varying PdZn-loading amount was first investigated. The results (Fig. 1) showed that the observed products of CO_2 hydrogenation included methanol (major) and HC (minor). The PdZn-loading amount of 16% (mass%) was optimal. Over the 16%$Pd_{0.085}Zn_1$/CNTs catalyst, the yield of methanol (i.e., the product of $X(CO_2$-hydr.) and $S(CH_3OH)$, symbolized as $Y(CH_3OH)$) reached 3.6%, while this value of the other five catalysts was successively 3.3%, 3.3%, 3.0%, 2.5% and 2.0%.

3.1.2. Pd/Zn molar ratio

The Pd/Zn molar ratio was then optimized. The results (Fig. 2) showed that the catalyst with Pd/Zn molar ratio of 0.1:1 had the highest catalytic activity. Over the 16%$Pd_{0.1}Zn_1$/CNTs catalyst, the observed $Y(CH_3OH)$ reached 3.9%, while this value of the other four catalysts was successively 3.7%, 3.6%, 3.1% and 2.9%.

3.2. Optimization of the reaction operation conditions

3.2.1. Reaction temperature

Reaction temperature has a significant effect on the conversion of CO_2 hydrogenation and the selectivity of methanol formation.

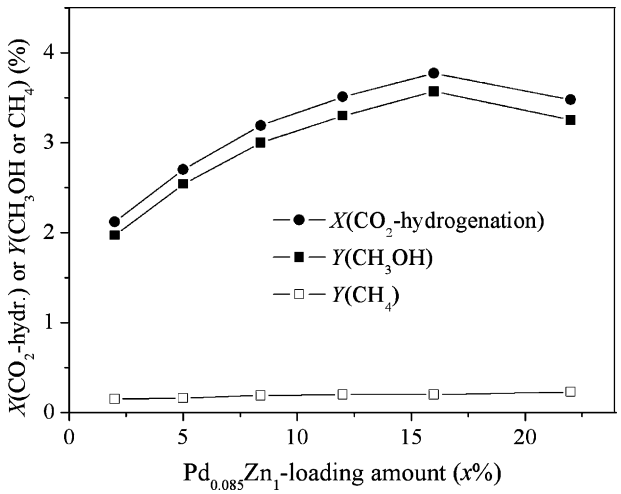

Fig. 1. Reactivity of CO_2 hydrogenation over the $x\%Pd_{0.085}Zn_1$/CNTs catalyst with varying $Pd_{0.085}Zn_1$-loading amounts; reaction conditions: 2.0 MPa, 523 K, $V(H_2)/V(CO_2)/V(N_2)$ = 69/23/8, GHSV = 1200 $ml_{STP}/(g \cdot h)$, 8 h.

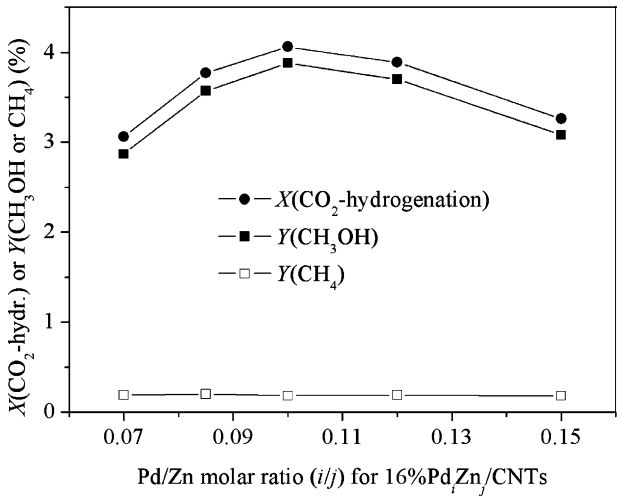

Fig. 2. Reactivity of CO_2 hydrogenation over the $16\%Pd_iZn_j$/CNTs catalyst with varying Pd/Zn molar ratio (i/j); reaction conditions are the same as in Fig. 1.

Reactivity of CO_2 hydrogenation to methanol was investigated under different reaction temperatures. The results were shown in Fig. 3. With the reaction temperature rising from 503 to 543 K, the conversion of CO_2 by "reverse-water–gas-shift (RWGS) reaction" monotonically increased, while the conversion of CO_2 hydrogenation, after reaching a maximum at 523 K, slowly descended. The increase of selectivity of CH_4 was accelerated when reaction temperature went up to 533 K and above, with simultaneous descend of CH_3OH selectivity. In order to obtain high space-time-yield (STY) of CH_3OH, 523 K was taken as the optimal operating temperature. Under the reaction conditions of 3.0 MPa, 523 K, $V(H_2)/V(CO_2)/V(N_2)$ = 69/23/8 and the correspondingly optimized GHSV (1800 $ml_{STP}/(g \cdot h)$), conversion of CO_2 hydrogenation reached 6.3%, with the selectivity of CH_3OH being 99.6% and the corresponding STY of CH_3OH being 37.1 $mg/(g \cdot h)$.

3.2.2. Reduction temperature

The temperature for the reduction of catalyst-precursor also has a marked effect on the performance of the catalyst for hydrogenation of CO_2 to methanol. As shown in Fig. 4, with the increase of reduction temperature for the $16\%Pd_{0.1}Zn_1$/CNTs, the conversion of CO_2-hydrogenation and the selectivity of methanol both

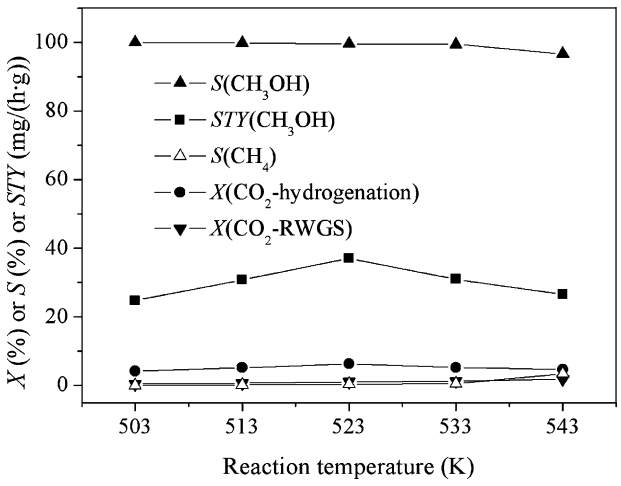

Fig. 3. Reactivity of CO_2 hydrogenation over the $16\%Pd_{0.1}Zn_1$/CNTs catalyst at different temperatures at: 3.0 MPa, $V(H_2)/V(CO_2)/V(N_2)$ = 69/23/8; GHSV = 1800 $ml_{STP}/(g \cdot h)$, 8 h.

increased, whereas the selectivity of methane declined correspondingly. The STY of methanol approached a plateau when the reduction temperature rising to 773 K and above. It follows that, in order to obtain both high CO_2 conversion and CH_3OH selectivity, it is necessary for the reduction temperature to elevate to 773 K for the $x\%Pd_iZn_j$/CNTs catalyst with $PdCl_2$ as precursor material.

The results of XRD measurements (Fig. 5) provided direct evidence for the formation of PdZn alloy upon the reduction of the CNT-supported Pd–ZnO catalyst. In the XRD patterns taken on the two samples of $16\%Pd_{0.1}Zn_1$/CNTs reduced to 773 and 823 K, the peak at $2\theta = 40.1^\circ$ (ascribed to the (1 1 1) reflection of metallic Pd_x^0) completely vanished, simultaneously with the two peaks at $2\theta = 41.2^\circ$ and 44.1° (due to the (1 1 1) and (2 0 0) reflections of PdZn alloy, respectively [18]) markedly enhanced, implying that PdZn alloy became the predominant Pd-containing crystallite-phase. This XRD result, in connection with the results of above catalyst tests (Fig. 4), strongly suggested that the catalytically active phase associated more closely with the selective formation of methanol was PdZn alloy, rather than metallic Pd, especially under reaction temperatures of $\geq$523 K. This is in line with the results reported previously on the ZnO-supported Pd catalyst [12].

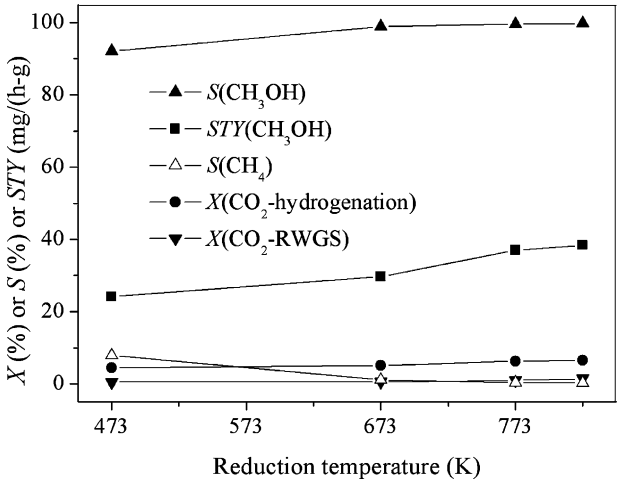

Fig. 4. Reactivity of CO_2 hydrogenation over $16\%Pd_{0.1}Zn_1$/CNTs catalyst reduced to different temperatures; reaction conditions for CO_2 hydrogenation are the same as in Fig. 3, except T = 523 K.

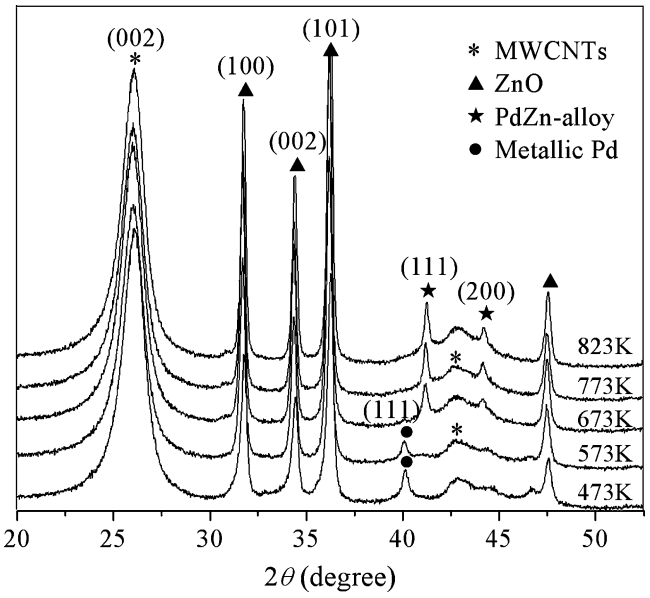

Fig. 5. XRD patterns of 16%$Pd_{0.1}Zn_1$/CNTs catalyst reduced to different temperatures; the temperatures to which the catalysts were reduced are indicated in the figure.

3.3. Reactivity over the $Pd_{0.1}Zn_1$ catalysts supported on different supporters

In order to gain a clear idea of the nature of promoting action by the CNTs, reactivity of CO_2 hydrogenation to methanol over the Pd–ZnO catalysts supported on CNTs(*p-type*), AC and γ-Al_2O_3, respectively, was evaluated and compared with that of the Pd–ZnO catalyst supported on the CNTs(*h-type*). The results (Fig. 6) showed that the supporter could significantly affect the reactivity of CO_2 hydrogenation. Under the reaction conditions of 3.0 MPa, 523 K, $V(H_2)/V(CO_2)/V(N_2) = 69/23/8$ and GHSV = 1800 $ml_{STP}/(g \cdot h)$, the conversion of CO_2 hydrogenation reached 6.30% over 16%$Pd_{0.1}Zn_1$/CNTs(*h-type*), while merely 5.86%, 4.19% and 3.57% over the counterparts supported on the CNTs(*p-type*), AC and γ-Al_2O_3, respectively (Fig. 6(A)); the corresponding methanol STY for the former was 37.1 mg/(h · g), which was 1.12, 1.51 and 1.93 times that (33.1, 24.5 and 19.2 mg/(h · g) of the latter three ones, successively (Fig. 6(B)).

In view of the difference in the specific surface area for different supporters, the optimization of $Pd_{0.1}Zn_1$-loading amount on the CNTs(*p-type*), AC and γ-Al_2O_3 supporters was done. The results showed that the optimal $Pd_{0.1}Zn_1$-loading amount was 22%, 35% and 20% for the CNTs(*p-type*), AC and γ-Al_2O_3, respectively. Over the 22%$Pd_{0.1}Zn_1$/CNTs(*p-type*), 35%$Pd_{0.1}Zn_1$/AC and 20%$Pd_{0.1}Zn_1$/γ-Al_2O_3 catalysts, the conversion of CO_2 hydrogenation attained 6.22%, 4.93% and 4.44%, respectively (Fig. 6(A)), under the same reaction conditions, with the corresponding methanol STY reached 35.0, 28.1 and 24.2 mg/(h · g), successively (Fig. 6(B)).

In order to compare the catalytic efficiency produced by unit site of Pd^0 exposed on the surface of the catalysts supported by the different supporters, the turnover-frequency (TOF), i.e., the number of CO_2-molecule hydrogenated on unit site of exposed Pd^0 per second (s^{-1}), was used as reference. Results from this study (see Table 1) showed that, for AC and γ-Al_2O_3 supported catalysts (at their optimal $Pd_{0.1}Zn_1$-loading amounts, 35%$Pd_{0.1}Zn_1$/AC and 20%$Pd_{0.1}Zn_1$/γ-Al_2O_3, respectively), their TOF (0.98×10^{-2} and 0.97×10^{-2} s^{-1}) were relatively low and close to each other. In contrast, the TOF for the two CNT-supported catalysts (at their optimal $Pd_{0.1}Zn_1$-loading amounts, 16%$Pd_{0.1}Zn_1$/CNTs(*h-type*) and 22%$Pd_{0.1}Zn_1$/CNTs(*p-type*)) were much higher (reaching 1.15×10^{-2} and 1.08×10^{-2} s^{-1}, respectively). Thus, it seemed to us that AC and γ-Al_2O_3 merely played the role as a catalyst-supporter, while the CNTs played dual roles as a catalyst support and a promoter.

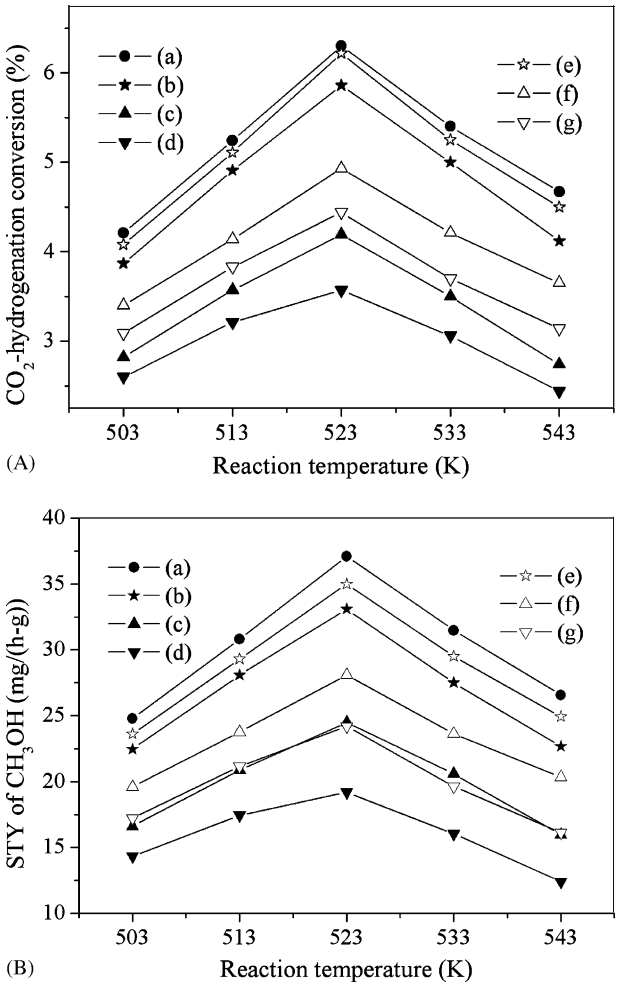

Fig. 6. Reactivity of CO_2 hydrogenation over the catalysts: (a) 16%$Pd_{0.1}Zn_1$/CNTs(*h-type*), (b) 16%$Pd_{0.1}Zn_1$/CNTs(*p-type*), (c) 16%$Pd_{0.1}Zn_1$/AC, (d) 16%$Pd_{0.1}Zn_1$/γ-Al_2O_3, (e) 22%$Pd_{0.1}Zn_1$/CNTs(*p-type*), (f) 35%$Pd_{0.1}Zn_1$/AC, and (g) 20%$Pd_{0.1}Zn_1$/γ-Al_2O_3; reaction conditions are the same as in Fig. 3.

The apparent activation energy (E_a) of CO_2 hydrogenation reactions on these catalysts was measured under the reaction conditions of 2.0 MPa, 503–543 K, $V(H_2)/V(CO_2)/V(N_2) = 69/23/8$; GHSV = 6000 $ml_{STP}/(g \cdot h)$, with mass transfer limitation ruled out. The results were shown in Fig. 7. The E_a observed on the 16%$Pd_{0.1}Zn_1$/CNTs(*h-type*) catalyst was 56.8 kJ/mol. This value was very close to 62.7 or 64.6 kJ/mol on the reference system supported on AC or γ-Al_2O_3. This indicated that using the CNTs in place of AC or γ-Al_2O_3 as support of the catalyst displayed little change in the E_a for CO_2 hydrogenation reactions, most likely implying that the use of the CNTs in place of AC or γ-Al_2O_3 as support did not alter the main reaction pathway of CO_2 hydrogenation.

3.4. Characterization of the catalysts

3.4.1. SEM and EDS characterization

Fig. 8 showed SEM image and energy dispersive spectrum (EDS) of the tested catalyst of 16%$Pd_{0.1}Zn_1$/CNTs(*h-type*). It can be seen from Fig. 8(a) that the Pd–Zn nanoparticles were smaller and were more evenly dispersed on the surface of the CNTs, in comparison with that of the tested catalysts of 35%$Pd_{0.1}Zn_1$/AC and 20%$Pd_{0.1}Zn_1$/γ-Al_2O_3 (Fig. 8(c) and (d)). The SEM/EDS analysis

Table 1
Reactivity of CO_2 hydrogenation to methanol over the supported Pd–ZnO catalysts.

Catalyst[a]	SSA (m^2/g)	Pd disper. (%)	SA_{Pd} (m^2/g)	$X(CO_2$-RWGS) (%)	$X(CO_2$-hydr.) (%)	TOF × 10^2 (s^{-1})	Selec. of CH_3OH (C%)	STY of CH_3OH (mg/(h · g))
16%$Pd_{0.1}Zn_1$/CNTs(*h-type*)	121	13.6	1.334	1.00	6.30	1.15	99.6	37.1
22%$Pd_{0.1}Zn_1$/CNTs(*p-type*)	133	10.4	1.392	1.48	6.22	1.08	95.2	35.0
35%$Pd_{0.1}Zn_1$/AC	515	5.59	1.220	1.48	4.93	0.98	96.5	28.1
20%$Pd_{0.1}Zn_1$/γ-Al_2O_3	110	8.93	1.114	0.58	4.44	0.97	92.1	24.2

[a] N_2-BET-SSA of the supporters: 135, 220, 830 and 217 (m^2/g) for CNTs(*h−type*), CNTs(*p-type*), AC and γ-Al_2O_3, respectively; reaction conditions: 3.0 MPa, 523 K, $V(H_2):V(CO_2):V(N_2)$ = 69:23:8, $GHSV_{outlet}$ = 1800 ml/(g · h).

demonstrated that carbon, Zn and Pd were the only three elements observed at the surface of catalyst, with the content at 94.52%, 4.91% and 0.57% (atomic percentage), the corresponding mass percentage being 74.97%, 21.00% and 4.03%, respectively (Fig. 8(b)).

3.4.2. XRD analysis

The XRD analysis of the tested catalysts showed that, in the position and shape of the main XRD features, there were few differences between the XRD patterns (Fig. 9(a)–(c)) taken on the catalysts supported on the three carbon-supporters, CNT(*h-type*), CNT(*p-type*) and AC, respectively, except for the features at $2\theta = 26.1^\circ$ and 43.1° for the two CNT-supported systems, which were due to the diffractions of (0 0 2) and (1 0 0) planes of graphite-like tube-wall of the CNTs [15,19]. In these three tested catalysts, the Pd and Zn components existed mainly in the forms of ZnO and PdZn alloy (with the observed XRD features at $2\theta = 31.8^\circ$/34.5°/36.3° and 41.2°/44.1°, respectively) [18], and the content of metallic Pd_x^0-phase was below the XRD-detection limit.

Being different from the aforementioned three catalysts supported on the carbon-supporters, on the γ-Al_2O_3-supported system, the observed XRD feature at $2\theta = 41.2^\circ$ ascribed to the PdZn alloy-phase was quite weak (Fig. 9(d)), implying that the diameters of PdZn alloy-particles were below ~2 nm, if existed. The other existing form of the Zn component was $(Zn_{0.5}Al_{0.7})Al_{1.7}O_4$, and the corresponding XRD features appeared at $2\theta = 31.6^\circ$/37.2°/45.3°, originated from the diffractions of (2 0 0), (3 1 1) and (4 0 0) planes of $(Zn_{0.5}Al_{0.7})Al_{1.7}O_4$, respectively [18]. Thus this implied that a strong interaction took place between ZnO and Al_2O_3, leading to the formation of $(Zn_{0.5}Al_{0.7})Al_{1.7}O_4$.

3.4.3. XPS analysis

XPS analysis of the tested catalysts revealed that certain differences existed among the catalysts supported on the different supporters in the valence-states of their surface Pd-species and the relative concentration. Fig. 10 showed the Pd(3*d*)-XPS spectra of the tested catalysts (undergoing the reduction at 773 K). The observed Pd($3d_{5/2}$) and ($3d_{3/2}$) XPS peaks appeared at ~335.6 and ~340.8 eV. These values are characteristics of Pd-species with mixed valences. With reference to Ref. [20] and through computer-fitting, it could be found that each of those Pd(3*d*)-XPS spectra involved the contribution from three kinds of surface Pd-species: Pd^0 (PdZn-alloy), Pd^{2+} (PdO) and Pd^{4+} (PdO_2) (see Fig. 10 and Table 2). At the surface of the tested 16%$Pd_{0.1}Zn_1$/CNTs(*h-type*) catalyst (reduced to 773 K), the molar percentage of Pd^0-species in the total Pd-amount reached 70.7 mol%, being 1.24, 1.36 and 1.44 times that (57.0, 52.1, 49.2 mol%) of the catalysts supported on the CNTs(*p-type*), AC and γ-Al_2O_3, respectively. It followed that the sequence of relative concentration of the Pd^0-species at the surface of these four catalysts was 16%$Pd_{0.1}Zn_1$/CNTs(*h-type*) > 22%$Pd_{0.1}Zn_1$/CNTs(*p-type*) > 35%$Pd_{0.1}Zn_1$/AC > 20%$Pd_{0.1}Zn_1$/γ-Al_2O_3. This sequence was in line with the observed sequence of reaction activity of CO_2 hydrogenation to methanol over these catalysts.

The use of ZnO-supported Pd as the catalysts for steam reforming of methanol and for the reverse reaction, CO_2 hydrogenation to methanol, has been reported by Iwasa et al. [12,21], Wang et al. [22] and Fukuhara et al. [23]. They observed that the original catalytic functions of metallic Pd were modified by the formation of PdZn alloys upon the reduction of the Pd–ZnO. Our above XPS results, in connection with the results of the above catalyst tests (Table 1) and XRD characterizations (Figs. 5 and 9), strongly supported the view that there existed some correlation between the surface Pd^0-species in form of PdZn alloys and the formation of methanol from CO_2 hydrogenation. The high concentration of the surface Pd^0-species in form of PdZn alloys was conducive to selective formation of methanol.

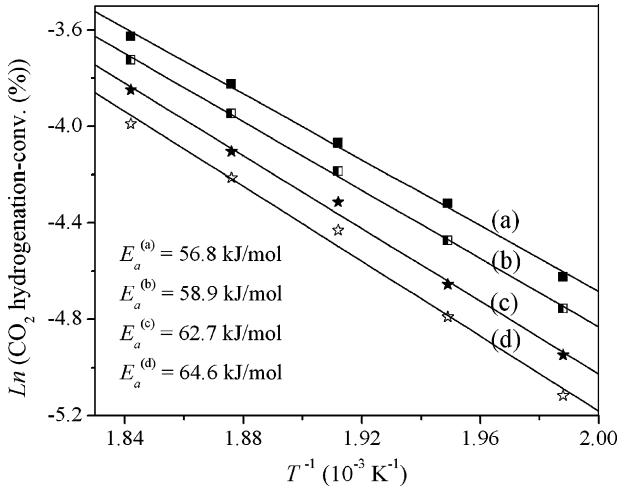

Fig. 7. Arrhenius plots of CO2 hydrogenation over the catalysts: (a) 16%$Pd_{0.1}Zn_1$/CNT(*h-type*); (b) 22%$Pd_{0.1}Zn_1$/CNT(*p-type*); (c) 35%$Pd_{0.1}Zn_1$/AC; (d) 20%$Pd_{0.1}Zn_1$/γ-Al_2O_3; taken at: 2.0 MPa, 503–543 K, $V(H_2)/V(CO_2)/V(N_2)$ = 69/23/8, GHSV = 6000 ml_{STP}/(g · h), 8 h.

3.4.4. H_2-TPD test

Recently, there has been increasing interest in the use of nanostructured carbon materials (such as: CNTs, carbon nanofibers, and mechanically milled graphite, etc.) as hydrogen sorbents. Ishikawa et al. [24] demonstrated that graphitized carbon black surfaces were capable of rapidly equilibrating H_2/D_2 mixtures. A dissociation rate of 2.5×10^{17} molecules/(s · m^2-ASA) was measured at ambient temperatures and pressures. The ASA (active surface area) was described in terms of atoms located at the edge positions on the graphite basal plane and was determined from the amount of oxygen able to chemisorb at these sites, regardless of the nature of the carbon material under investigation. Our previous H_2-TPD investigation [25] showed that hydrogen adsorption on the CNTs can occur at ambient temperatures and pressures, and that the desorbed product was almost exclusively H_2 at temperatures lower than 723 K, while it included CH_4, C_2H_4 and C_2H_2, in addition to H_2, at temperatures of 773 K and above. This implies that H_2 adsorption on the CNTs may be in two forms: associative (molecular state) and dissociative (atomic state), as having been evidenced in our Raman spectroscopic study of H_2/MWCNTs adsorption system [19].

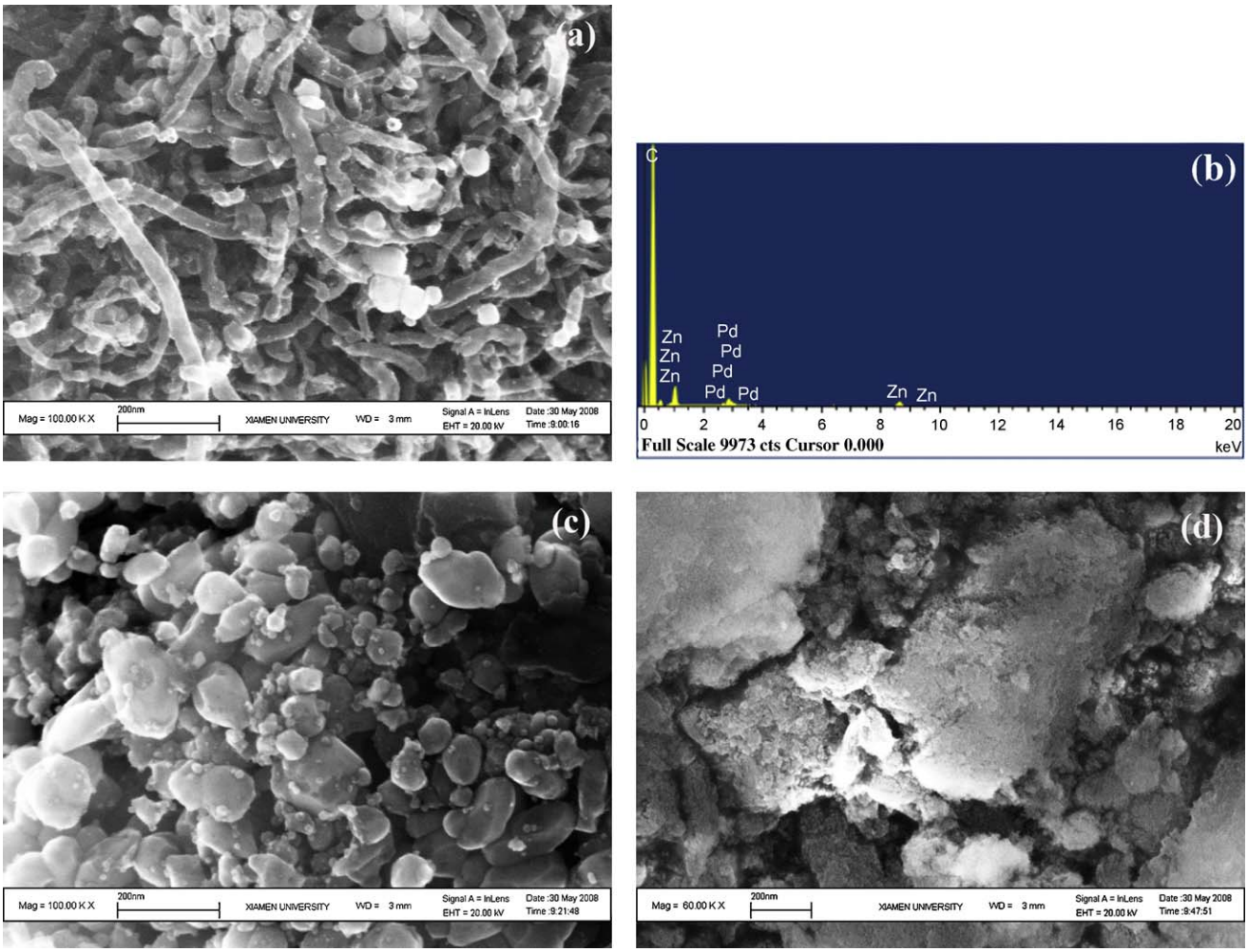

Fig. 8. SEM image (a) and energy dispersive spectrum (EDS) (b) of 16%$Pd_{0.1}Zn_1$/CNTs(*h-type*); SEM images of: (c) 35%$Pd_{0.1}Zn_1$/AC and (d) 20%$Pd_{0.1}Zn_1$/γ-Al_2O_3.

Fig. 11 showed the TPD profiles of hydrogen adsorbed on the pre-reduced catalysts supported on the CNTs(*h-type*), CNTs(*p-type*), AC and γ-Al_2O_3, respectively. Both of H_2-TPD profiles (Fig. 11(a) and (b)) taken on the catalysts supported by the two types of CNTs contained a lower temperature peak (peak I, 323–543 K) and a higher temperature peak (peak II, 543–623 K). Peak I resulted from the desorption of weakly adsorbed hydrogen-species (probably including molecularly adsorbed hydrogen H_2(a) and weak-dissociatively adsorbed H-species), and peak II was attributed to the desorption of strongly adsorbed H-species, perhaps dissociatively chemisorbed hydrogen H(a). As compared with that of the catalysts supported on the two types of CNTs, the shape of the H_2-TPD peaks (Fig. 11(c) and (d)) of the AC (or γ-Al_2O_3)-supported catalysts was relatively broad (spanning from 323 to 623 K), and their intensity was much lower. The relative area-intensities of the H_2-TPD peaks for these catalyst samples were estimated. The ratio of the obtained relative area-intensities was S(16%$Pd_{0.1}Zn_1$/CNTs(*h-type*))/S(22%$Pd_{0.1}Zn_1$/CNTs(*p-type*))/S(35%$Pd_{0.1}Zn_1$/AC)/S(20%$Pd_{0.1}Zn_1$/γ-Al_2O_3) = 100/81/26/21. This suggested that the sequence of increasing concentration of H-adspecies at the surface of functioning catalysts was 16%$Pd_{0.1}Zn_1$/CNTs(*h-type*) > 22%$Pd_{0.1}Zn_1$/CNTs(*p-type*) > 35%$Pd_{0.1}Zn_1$/AC > 20%$Pd_{0.1}Zn_1$/γ-Al_2O_3, in line with the observed sequence of reaction activity over these catalysts for the CO_2 hydrogenation to methanol.

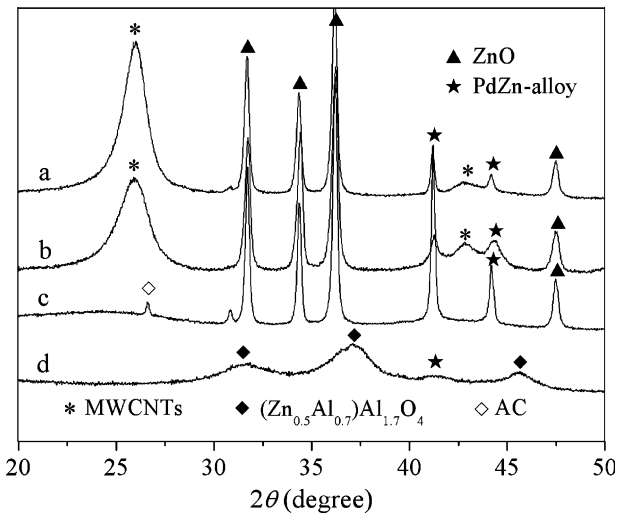

Fig. 9. XRD patterns of the tested catalysts: (a) 16%$Pd_{0.1}Zn_1$/CNTs(*h-type*); (b) 22%$Pd_{0.1}Zn_1$/CNTs(*p-type*); (c) 35%$Pd_{0.1}Zn_1$/AC; (d) 20%$Pd_{0.1}Zn_1$/γ-Al_2O_3.

3.5. Nature of promoter action by the CNTs

The results of metallic Pd surface area (Pd^0-SA) measurement showed that Pd exposed area of the 16%$Pd_{0.1}Zn_1$/CNTs(*h-type*) catalyst reached 1.334 m^2/g, which was 9.3% and 19.7% higher than those (i.e., 1.220 and 1.114 m^2/g) of the AC- and γ-Al_2O_3-supported

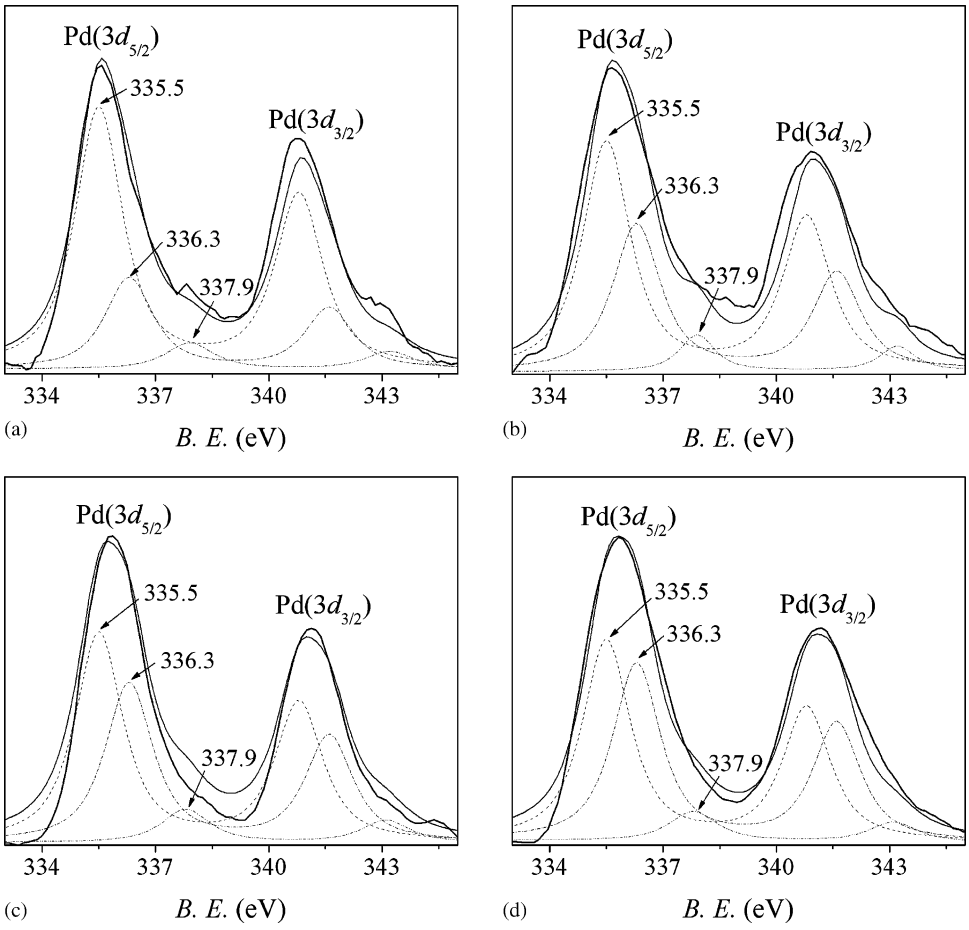

Fig. 10. XPS spectra of Pd(3*d*) of the tested catalysts: (a) 16%$Pd_{0.1}Zn_1$/CNTs(*h-type*); (b) 22%$Pd_{0.1}Zn_1$/CNTs(*p-type*); (c) 35%$Pd_{0.1}Zn_1$/AC; (d) 20%$Pd_{0.1}Zn_1/\gamma$-Al_2O_3.

reference catalysts, respectively (see Table 1). The increment of Pd surface area was undoubtedly in favor of enhancing the specific activity of the catalyst. Nevertheless, it would be difficult to be convinced that the 32% or 53% increase in methanol STY (i.e., 37.1 mg/(h · g) vs. 28.1 mg/(h · g) for the 16%$Pd_{0.1}Zn_1$/CNTs(*h-type*) vs. 35%$Pd_{0.1}Zn_1$/AC or 37.1 mg/(h · g) vs. 24.2 mg/(h · g) for the 16%$Pd_{0.1}Zn_1$/CNTs(*h-type*) vs. 20%$Pd_{0.1}Zn_1/\gamma$-Al_2O_3) was solely attributed to the difference in their Pd surface area. Besides, the difference in the surface areas could hardly justify the 17% and 18% increase of the TOF, i.e., from 0.98×10^{-2} and 0.97×10^{-2} s^{-1} for AC- and γ-Al_2O_3-supported systems, respectively, going up to 1.15×10^{-2} s^{-1} for the CNTs(*h-type*)-supported system (see Table 1).

Therefore, it appears that the high activity of the CNTs(*h-type*)-supported catalyst for CO_2 hydrogenation to methanol is also closely associated with the peculiar structure and properties of the CNTs as supporter. In view of chemical catalysis, in addition to its high mechanical strength, nanosize channel, sp^2-C constructed surface and graphite-like tube-wall, the excellent performance of the CNTs in hydrogen-adsorption and electron transport is also very attractive. It could be inferred from the above TPD investigations that there would exist a considerably greater

Table 2
XPS binding energies and relative contents of the Pd-species with different valence-states at the surface of tested catalysts.

Catalyst	E_b (Pd($3d_{5/2}$)) (eV)			Relative content (mol%)		
	Pd^0	Pd^{2+} (PdO)	Pd^{4+} (PdO_2)	Pd^0	Pd^{2+} (PdO)	Pd^{4+} (PdO_2)
16%$Pd_{0.1}Zn_1$/CNTs(*h-type*)	335.5	336.3	337.9	70.7	25.8	3.5
22%$Pd_{0.1}Zn_1$/CNTs(*p-type*)	335.5	336.3	337.9	57.0	36.4	6.6
35%$Pd_{0.1}Zn_1$/AC	335.5	336.3	337.9	52.1	40.1	7.8
20%$Pd_{0.1}Zn_1/\gamma$-Al_2O_3	335.5	336.3	337.9	49.2	43.0	7.8

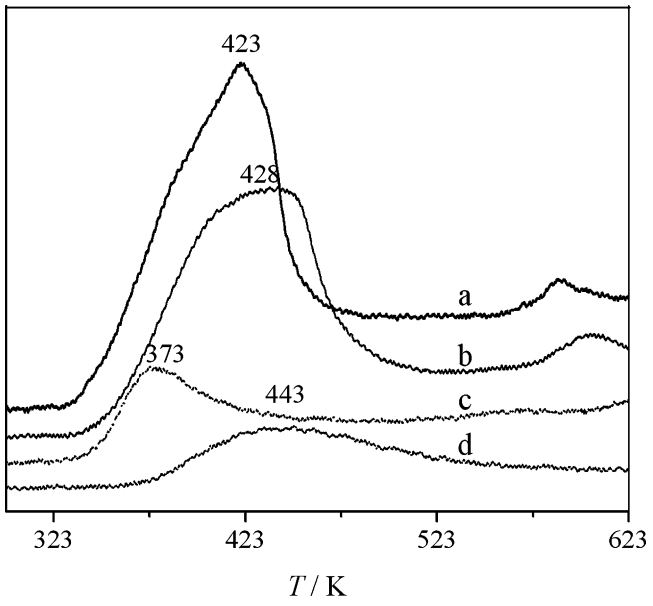

Fig. 11. TPD profiles of H_2 adsorption on the pre-reduced catalysts: (a) 16%$Pd_{0.1}Zn_1$/CNTs(*h-type*); (b) 22%$Pd_{0.1}Zn_1$/CNTs(*p-type*); (c) 35%$Pd_{0.1}Zn_1$/AC; (d) 20%$Pd_{0.1}Zn_1/\gamma$-Al_2O_3.

amount of hydrogen-adspecies on the CNT supporter under the condition of CO_2 hydrogenation used in the present study. This would generate a micro-environment with higher stationary-state concentration of hydrogen-adspecies. Those active H-adspecies could be easily transferred to Pd active sites via the CNT-promoted hydrogen spillover, thus increasing the rate of the surface hydrogenation reactions. This was very similar to the scenario in synthesis of methanol and higher alcohols from syngas over the CNTs(*h-type*)-promoted Cu–ZnO–Al_2O_3 [26,27], Co–Cu [28] and Co–Mo–K [29] catalysts, respectively.

In comparison with the CNTs(*p-type*), the CNTs(*h-type*) possess more active surface (with more dangling bonds) [15,19], and thus, higher capacity for adsorption-activation of H_2 [19], which make their promoting action more remarkable (see Table 1 and Fig. 11).

3.6. Design and preparation of highly active CNT-promoted co-precipitated catalyst

Making use of the promoter action by the CNTs, highly active and practical CNT-promoted Pd–ZnO catalysts, Pd_iZn_j–*x*%CNTs, have been designed and prepared by co-precipitation method. The experiment results displayed that appropriate incorporation of a minor amount of the CNTs into the Pd_iZn_j can significantly advance the catalyst activity for CO_2 hydrogenation to methanol. Over a co-precipitated $Pd_{0.085}Zn_1$–9%CNTs catalyst under the reaction conditions of 5.0 MPa, 533 K, $V(H_2)/V(CO_2)/V(N_2) = 69/23/8$ and GHSV = 8000 $ml_{STP}/(h \cdot g)$, the observed TOF reached $4.33 \times 10^{-2}\ s^{-1}$, which is 18.3 times that ($2.36 \times 10^{-3}\ s^{-1}$) of the co-precipitated Cu–ZrO_2 catalyst under the same reaction condition [30]. The selectivity of methanol in the CO_2 hydrogenation products reached 100%, with corresponding STY of methanol reaching 148 $mg/(h \cdot g)$. The work is in progress.

4. Concluding remarks

(1) In the developed CNT-supported Pd–ZnO catalysts for CO_2 hydrogenation to methanol, the CNTs played dual roles as a catalyst supporter and a promoter.
(2) Using the CNTs in place of AC or γ-Al_2O_3 as the catalyst support resulted in an increase of the relative content, at surface of the functioning catalyst, of the catalytically active Pd^0-species closely associated with the methanol generation.
(3) The CNT-supported Pd–ZnO catalysts could reversibly adsorb a greater amount of hydrogen, which would be in favor of generating a micro-environment with higher concentration of active H-adspecies at the surface of the functioning catalyst, thus increasing the rate of surface hydrogenation reactions.
(4) The promoting action of the Herringbone-type CNTs was more remarkable, in comparison with that of the Parallel-type CNTs.

For better understanding of the nature of the promoting action by CNTs, further studies, especially *in situ* characterization of reaction intermediates under the actual reaction conditions would be highly desired.

Acknowledgments

The authors are grateful for the financial supports from National Natural Science Foundation (Projects No. 20590364) and National Basic Research (“973”) Project (Project No. 2005CB221403) of China.

References

[1] T. Tagawa, G. Pleizier, Y. Amenomiya, Appl. Catal. 18 (1985) 285.
[2] Y. Amenomiya, Appl. Catal. 30 (1987) 57.
[3] R.A. Koeppel, A. Baiker, C. Schild, W. Wokaun, Stud. Surf. Sci. Catal. 63 (1991) 59.
[4] N. Kanoun, M.P. Astier, G.M. Pajonk, Catal. Lett. 15 (1992) 231.
[5] M. Sahibzada, D. Chadwick, I.S. Metcalfe, Catal. Today 29 (1996) 367.
[6] I. Melian-Cabrera, M. Lopez Granados, P. Terreros, J.L.G. Fierro, Catal. Today 45 (1998) 251.
[7] J. Toyir, P.R. de la Piscina, J.L.G. Fierro, N. Homs, Appl. Catal. B: Environ. 29 (2001) 207.
[8] I. Melian-Cabrera, M. Lopez Granados, J.L.G. Fierro, J. Catal. 210 (2002) 285.
[9] L. Fan, K. Fujimoto, J. Catal. 150 (1994) 217.
[10] T. Fujitani, M. Saito, Y. Kanai, T. Watanabe, J. Nakamura, T. Uchijima, Appl. Catal. A: Gen. 125 (1995) L199.
[11] L. Fan, K. Fujimoto, J. Catal. 172 (1997) 238.
[12] N. Iwasa, H. Suzuki, M. Terashita, M. Arai, N. Takezawa, Catal. Lett. 96 (2004) 75.
[13] K.P. de Jong, J.W. Geus, Catal. Rev. Sci. Eng. 42 (2000) 481.
[14] P. Serp, M. Corrias, P. Kalck, Appl. Catal. A: Gen. 253 (2003) 337.
[15] H.B. Zhang, G.D. Lin, Y.Z. Yuan, Curr. Top. Catal. 4 (2005) 1.
[16] P. Chen, H.B. Zhang, G.D. Lin, Q. Hong, K.R. Tsai, Carbon 35 (1997) 1495.
[17] P.A. Webb, C. Orr, Analytical Methods in Fine Particle Technology, Micromeritics Instrument Corporation, Norcross, GA, USA, 1997, p. 260.
[18] XRD data bank attached to X'Pert PRO X-ray Diffractometer, PANalytical, The Netherlands, 2003.
[19] H.-B. Zhang, G.-D. Lin, Z.-H. Zhou, X. Dong, T. Chen, Carbon 40 (2002) 2429.
[20] J.F. Moulder, W.F. Stickle, P.E. Sobol, K.D. Bomben, Handbook of X-ray Photoelectron Spectroscopy—A Reference Book of Standard Spectra for Identification and Interpretation of XPS Data, Physical Electronics Inc., Eden Prairie, MN, USA, 1995
[21] N. Iwasa, S. Masuda, N. Ogawa, N. Takezawa, Appl. Catal. A: Gen. 125 (1995) 145.
[22] Y. Wang, J. Zhang, H. Xu, Chin. J. Catal. 27 (2006) 217.
[23] C. Fukuhara, Y. Kamata, A. Igarashi, Appl. Catal. A: Gen. 330 (2007) 108.
[24] Y. Ishikawa, L.G. Austin, D.E. Brown, P.L. Walker Jr., in: P.L. Walker, Jr., P.A. Thrower (Eds.), Chemistry and Physics of Carbon, vol. 12, American Carbon Society, Marcel Dekker, New York, 1975, p. 39.
[25] Z.-H. Zhou, X.-M. Wu, Y. Wang, G.-D. Lin, H.-B. Zhang, Acta Phys. Chim. Sinica 18 (2002) 692.
[26] H.-B. Zhang, X. Dong, G.-D. Lin, Y.-Z. Yuan, P. Zhang, K.-R. Tsai, in: C.J. Liu, R.G. Mallinson, M. Aresta (Eds.), Proceedings of the ACS Symp. Ser. 852, American Chemical Society, Washington, DC, (2003), p. 195.
[27] X. Dong, H.-B. Zhang, G.-D. Lin, Y.-Z. Yuan, K.-R. Tsai, Catal. Lett. 85 (2003) 237.
[28] H.-B. Zhang, X. Dong, G.-D. Lin, X.-L. Liang, H.-Y. Li, Chem. Commun. (2005) 5094.
[29] X.-M. Wu, Y.-Y. Guo, J.-M. Zhou, G.-D. Lin, X. Dong, H.-B. Zhang, Appl. Catal. A: Gen. 340 (2008) 87.
[30] H. Li, G.-D. Lin, H.-B. Zhang, J. Xiamen Univ. (Nat. Sci. Ed.) 47 (2008) 765.